Journal of Magnetism and Magnetic Materials 321 (2009) 2210–2215

Contents lists available at ScienceDirect

Journal of Magnetism and Magnetic Materials

journal homepage: www.elsevier.com/locate/jmmm

Current perspectives

Raman and magnetic susceptibility studies of hexagonal elpasolite $Cs_2NaAlF_6:Cr^{3+}$

L.P. Sosman [a,*], F. Yokaichiya [b], H.N. Bordallo [b]

[a] Instituto de Física, UERJ, Rua São Francisco Xavier, 524, 20550-900 Rio de Janeiro, Brazil
[b] Helmholtz-Zentrum Berlin für Materialien und Energie GmbH, Gliniecker Str., 100, 14109 Berlin, Germany

ARTICLE INFO

Article history:
Received 16 November 2008
Received in revised form
18 January 2009
Available online 3 February 2009

PACS:
63.20.Pw
78.30.−j
42.70.Gi

Keywords:
Polarized Raman
Elpasolite
Chromium doping
Magnetic correlation

ABSTRACT

Polarized Raman scattering spectra of distorted $R\bar{3}m$ elpasolites Cs_2NaAlF_6 with a Cr^{3+} content of 0.1, 0.5 and 3.0 at% have been studied at both room temperature and 16 K. A shoulder located near the very intense band assigned to the AlF_6^{3-} A_{1g} mode indicates that the guest ion causes only small perturbations to the host lattice. Magnetic susceptibility measurements performed on the 0.1, 0.5, 3, 10 and 50 at% samples show that for particular concentrations the Cr^{3+} ions are not isolated, but participate to inter and/or intra-cluster magnetic exchange.

© 2009 Elsevier B.V. All rights reserved.

1. Introduction

Cs_2NaAlF_6 is a perovskite-related compound belonging to the A_2BMX_6 family of materials, where A, B and M are metal cations or more complex molecular ions and X is a halogen anion or an oxygen atom. These minerals have been classified as part of the elpasolites group. In doped elpasolites, the physical properties are related to point defects that arise during the compound's formation process by the insertion of interstitials impurities into the host lattice. In insulating elpasolites doped with transition-metals such as Cr, Fe, Co, Ni and Mn, the most important optical features are broad emission and absorption bands in the visible and near-infrared regions [1–4]. These bands allow the materials to function in a wide class of applications ranging from room temperature solid state lasers to special paper sheets to oriented dosimeter chips [5–9] for radiological protection.

$Cs_2NaAlF_6:Cr^{3+}$ crystallizes in a hexagonal structure having $R\bar{3}m$ symmetry, with $Z=6$ [10], see Fig. 1. In this space group, the Al occupy octahedral 3*a* or 3*b* position (with the local symmetry D_{3d}), while the Na anion resides in the 6*c* position (with the local symmetry C_{3v}). Previous investigation of $Cs_2NaAlF_6:Cr^{3+}$samples with various Cr^{3+} concentrations demonstrated phase pure samples, whose X-ray diffraction patterns were indexed with the same space group [10]. It was shown that there were no additional Bragg peaks or features that would suggest that the replacement of Al for Cr resulted in any phase separations or impurities, indicating a clear $Cs_2NaAl_{1-x}Cr_xF_6$ solid solution. The incorporation of Cr^{3+} ions into the Al site of Cs_2NaAlF_6 results in the formation of local $[CrF_6]^{3-}$ centers, which couple to the host lattice through electron–phonon (el–ph) interactions; observation of host lattice contributions to the vibrational sidebands can be attributed to the strength of the el–ph interaction. In fact, when the fluorescence spectra of Cr^{3+}-doped in two similar hexafluoride, Cs_2NaAlF_6 and Cs_2NaGaF_6, are compared [11], one can verify that the energy splitting of the $t_{2u}(\pi)$ mode associated with site I (site 3a in Refs. [10,12]) is larger in Cs_2NaAlF_6 than in Cs_2NaGaF_6. For site II (site 3b in Refs. [10,12]), this splitting also occurs in $Cs_2NaAlF_6:Cr^{3+}$, but it is not observed in the $Cs_2NaGaF_6:Cr^{3+}$ spectrum. Another interesting comparison concerns the $t_{2g}(\pi)$ vibronic origin. This mode is well resolved in the spectrum of the aluminate, while it is partially resolved in the gallate. These results indicate that the degree of local distortion on the sites occupied by Cr^{3+} ions is greater in $Cs_2NaAlF_6:Cr^{3+}$ compared to related compounds. Most recent electron paramagnetic resonance and electron-nuclear double resonance experiments support the spectroscopic results [13].

A direct insight into the electronic behavior of these condensed phase systems can be obtained using phonon analysis. In this

* Corresponding author at: Tel./Fax: 55 21 2587 7447.
E-mail address: sosman@uerj.br (L.P. Sosman).

0304-8853/$ - see front matter © 2009 Elsevier B.V. All rights reserved.
doi:10.1016/j.jmmm.2009.01.026

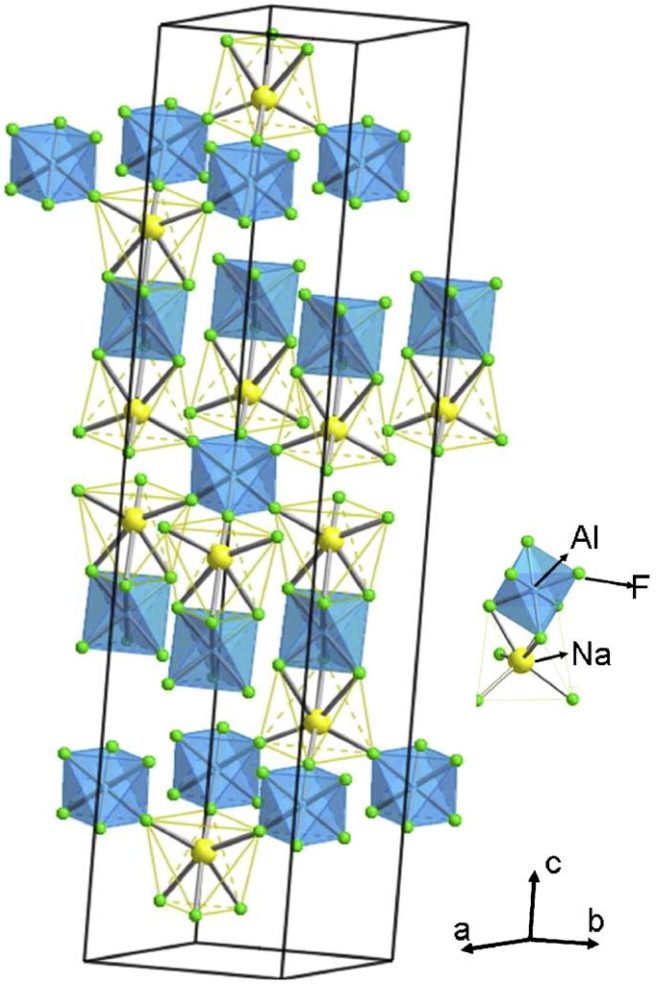

Fig. 1. Crystal structure projections for Cs_2NaAlF_6. (a) The transparent polyhedra represents NaF_6 and the semi-transparent frame, the $Al(Cr)F_6$ polyhedra.

paper, we report polarized single crystal Raman spectroscopy to probe in detail the site symmetry distortions in Cs_2NaAlF_6:Cr^{3+} with Cr^{3+}doping of 0.1, 0.5 (already reported in 10) and 3.0 at%. Moreover, the dilution of the magnetic Cr^{3+} ions can, to some extent, induce inter and/or intra-cluster magnetic exchange [14]. Thus, magnetic measurements were done in the temperature region between 2 K and room temperature in Cs_2NaAlF_6 with Cr^{3+} doping ranging from 0.1 to 50 at%.

2. Experimental

Single crystal of the Cs_2NaAlF_6:Cr^{3+} with 0.1, 0.5, 3, 10 and 50 at% Cr^{3+} doping were prepared by hydrothermal methods [15], producing crystals with a plate morphology with the [0 0 1] plane as the dominant face; a natural tendency of these materials.

Polarized, single crystal Raman scattering measurements were collected in a back-scattering configuration, using excitation 514 nm, 3.0 mW provided by a 10 W Spectra-Physics 2200 Ar^+ ion laser. Temperature control at $\pm$1.0 K was provided by an APD Heli-Tran cryostat controlled by an SI 9620-1 temperature controller.

To evaluate the magnetic contribution, temperature magnetization measurements were made in a randomly oriented (60–120 mg) samples with 0.1, 0.5, 3, 10 and 50 at% Cr^{3+}doping using a SQUID magnetometer (Quantum Design MPMS). In addition, measurements of the magnetic field dependence of the magnetization were made at 2 K for all samples.

3. Results and discussion

Raman measurements were obtained from the crystals mounted in three different orientations, $\langle z|xx|z\rangle$, $\langle z|yy|z\rangle$ and $\langle z|xy|z\rangle$. In such orientations, incident and observed light are parallel to the z-direction, while the measurements are made using either not-crossed or crossed polarization, respectively. A schematic view of the crossed polarization analysis $\langle z|xy|z\rangle$ is given in Fig. 2.

Using group analysis methods [16], the vibrational modes are represented by 7 A_{1g} (zz, xx+yy)+9 E_g(xy, xz, yz, xx−yy)+2 A_{1u}+9 A_{2u}+11 E_u+2 A_{2g}. The Raman tensor components in which the corresponding vibrations are active are indicated in parentheses. The A_{2g} are silent modes.

It is worth noting that the positions of the vibrational bands in several elpasolites systems are similar [17–22]. Of the sixteen Raman-active modes, only five (two A_{1g} and three E_g) are normally observed between 200 and 600 cm^{-1}. In fluorides with elpasolites structure, the A_{1g} modes arise from F-ion stretching modes in the D_{3d} factor group for the crystal and the E_g modes corresponding to motions of alkaline cations and F ions in the xy-plane.

The obtained Raman spectra are shown in Fig. 3. As the laser radiation is within the absorption region of the Cr^{3+}, the background is expected to be higher [23]. The mode assignments, given in Table 1, could be made as follows. The intensity of an MX_6^{3-} anion normally follows the order $I(A_{1g}) > I(E_g)$ [2,24], so the mode located at 520 cm^{-1}, which intensity is much weaker in the

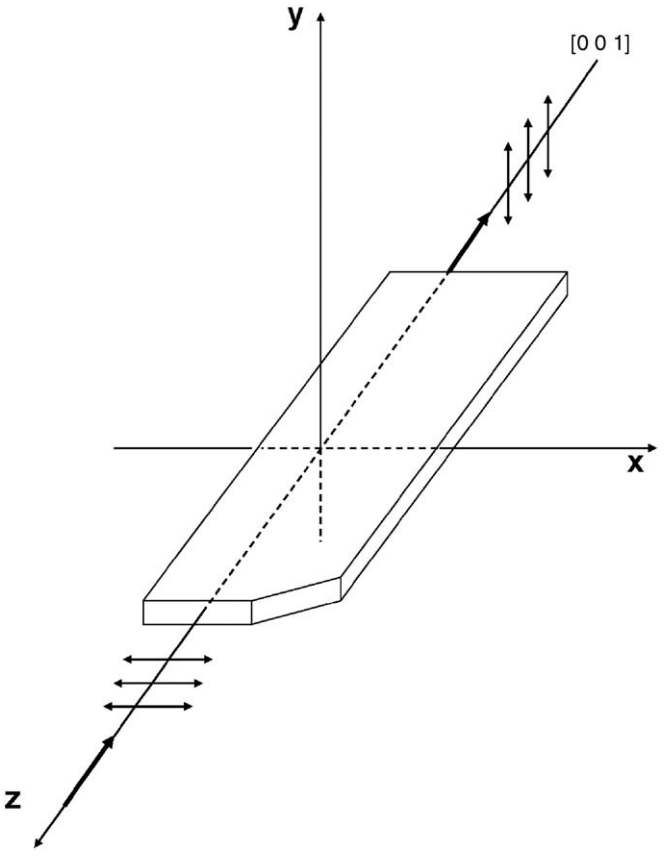

Fig. 2. Schematic view of the orientation $\langle z|xy|z\rangle$ for the Cs_2NaAlF_6:Cr^{3+}single crystal used in the polarized Raman scattering measurements. Note that O_{xyz} is the orthogonal referential in which Raman tensors are defined.

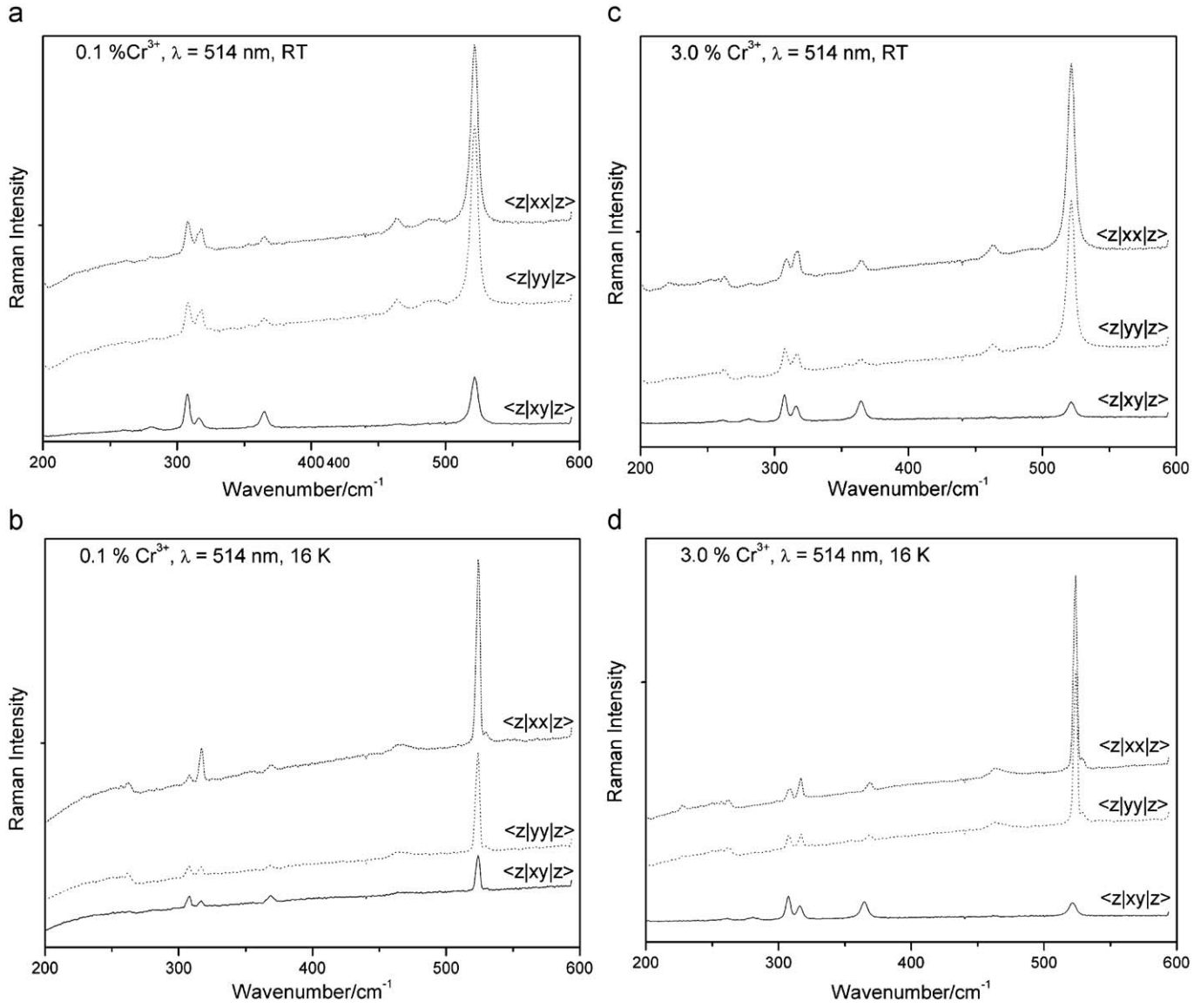

Fig. 3. Polarized Raman spectra of Cs_2NaAlF_6 at room temperature (*a* and *c*) and at 16 K (*b* and *d*), with 0.1% and 3.0% Cr^{3+}, respectively.

Table 1
Phonon wavenumber/cm^{-1} of Raman-active modes of vibration in Cs_2NaAlF_6:Cr^{3+} at room temperature (RT) and 16 K.

Mode symmetry O_h	Mode symmetry D_{3d}	Wavenumber/cm^{-1} (RT) $\pm 3/cm^{-1}$	Wavenumber/cm^{-1} (16 K) $\pm 3/cm^{-1}$
T_{2g} (ν_5)	E_g–?	307	308
T_{2g} (ν_5)	A_{1g}	310 [10]	
T_{2g} (ν_5)	E_g–?	316	316
E_g (ν_2)	E_g	364	370
A_{1g} (ν_1)	A_{1g}	520	525

Due to the distortion of the octahedral, the mode T_{2g} (ν_5) is predicted around 300 cm^{-1}. Thus, only one of the E_g bands arises from an internal motion of AlF_6^{3-} octahedral.

crossed polarized spectra, was assigned to the AlF_6^{-3} polyhedron vibrational mode A_{1g}. The remaining modes located at 307, 316 and 364 cm^{-1} are E_g modes. Since the AlF_6^{3-} is in a slightly distorted octahedral coordination (D_{3d}), its internal modes will rise as a result of splitting the three internal modes in an ideal O_h (A_{1g} (ν_1); E_g (ν_2) and T_{2g} (ν_5)) site symmetry found in the F3m3-type elpasolites. To the same extent, the octahedral vibrational modes are interrelated: $\nu_1^2 = \nu_2^2 + 3/2\nu_5^2$. So from the values for the ν_1 and ν_2 octahedral modes of about 520 and 364 cm^{-1}, respectively, one would expect a $\nu_5 \sim 304\,cm^{-1}$. Thus, either one of the E_g modes (307 or 316 cm^{-1}) or the A_{1g} mode (310 cm^{-1}, clearly seen in 10) is also an internal mode of the AlF_6^{3-}

Furthermore, as is clearly depicted in Fig. 4(a–c), a weak sideband, whose resolution increases on cooling (see Fig. 3) is observed at 528 cm^{-1}. Based on previous luminescence spectra [11], a well-defined vibrational structure is associated with normal modes of the octahedral complex $[CrF_6]^{3-}$. Thus, the small sideband can be unambiguously ascribed to effects arising from local perturbation of the Cr^{3+} in the lattice. Considering that the intensity at a given frequency in the sideband depends on the magnitude of the electron–phonon coupling [25], one can use this information to hypothesize on the variation of quantum yield as a function of doping. A poor quantum yield will be related to the increasing non-radiative relaxation pathways, due to the increasing el–ph coupling strength [26]. Thus, the Raman spectra were

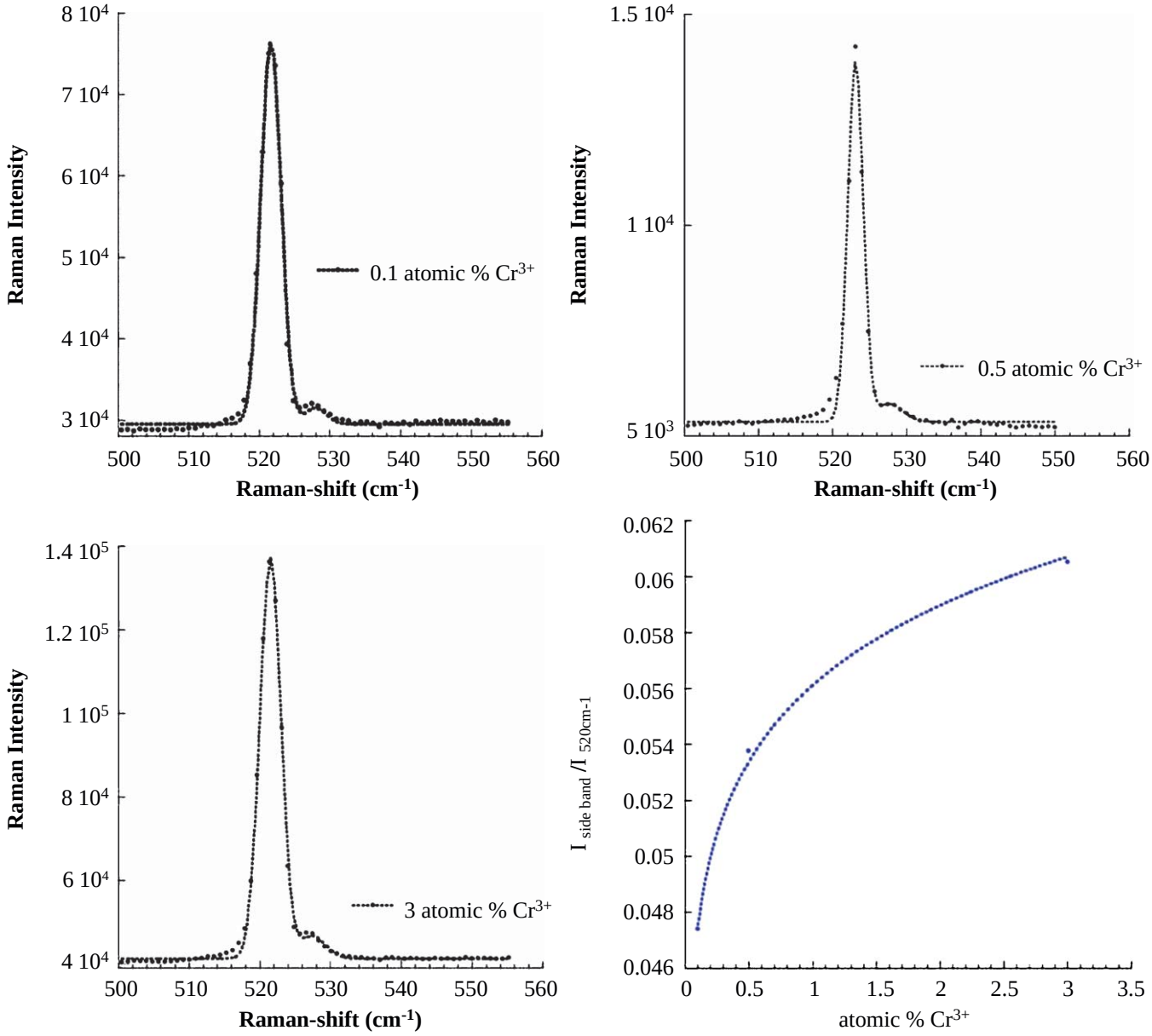

Fig. 4. Evolution of the sideband, assigned in the text as the local mode, as a function of Cr^{3+} concentration (a) 0.1, (b) 0.5 and (c) 3.0 at% Cr^{3+}. The evolution of obtained relative intensities of the side-bands as a function of atomic % is given in (d).

fitted between 500 and 550 cm^{-1}, Fig. 4(d), and the obtained relative intensities of the sidebands as a function of atomic % calculated. These vibrational results encourage a deeper investigation of the luminescence properties of this sample, as a function of doping level. The interest in this system is linked to previous results [11,23] using 0.5 at% Cr^{3+} doping, which show a quantum yield of about 0.4 at room temperature and a very intense and broad fluorescence band in the visible and infrared regions. In this respect, further luminescence measurements are needed to verify whether the quantum yield is maximized for a concentration lower or higher than 0.5 at% Cr^{3+}.

The temperature dependence of the reciprocal magnetic susceptibility of Cs_2NaAlF_6:Cr^{3+} with 0.1, 0.5, 3, 10 and 50 at% Cr^{3+} is presented in Fig. 5. For 0.1, 0.5 and 3 at% Cr^{3+}, the magnetic susceptibility measurements show that the paramagnetic contribution of the Cr^{3+} becomes more significant than the diamagnetism of the host lattice at different temperatures, similar behavior was reported by Chepeleva et al. [27], for incorporated Cr^{3+} in chalcogenide glasses. On the other hand, a Curie-Weiss law, $\chi = (C/T-\theta)$ is clearly followed by the 10 and 50 at% Cr^{3+} samples. As shown in Fig. 5(e), from the inverse susceptibility we obtained an effective Bohr magnetron number per chromium ion of 0.59 μ_B [28], giving $S = \frac{1}{2}$ in the paramagnetic state. To understand such result, we must consider that in this particular structure, the Cr^{3+} ion occupies a trigonal site with D_{3d} symmetry, and accordingly the enhancement of the trigonal component of the local crystal field is allowed. While Cr^{3+} in octahedral coordination has only one electron configuration with high spin (HS) states, Cr^{3+} in tetrahedral coordination may have the high spin or the LS states. Indeed, based on luminescence data [23] and crystal field modeling [29] LS state with $S = \frac{1}{2}$ is found in Cs_2NaAlF_6:0.5% Cr^{3+} at low temperatures (where as discussed above, the system is paramagnetic). Moreover, the existence of antiferromagnetic (AFM) correlations between Cr^{3+} centers in the 50% Cr^{3+}-doped sample is indicated by the decreasing nature of χT vs. T (see the inset of Fig. 5).

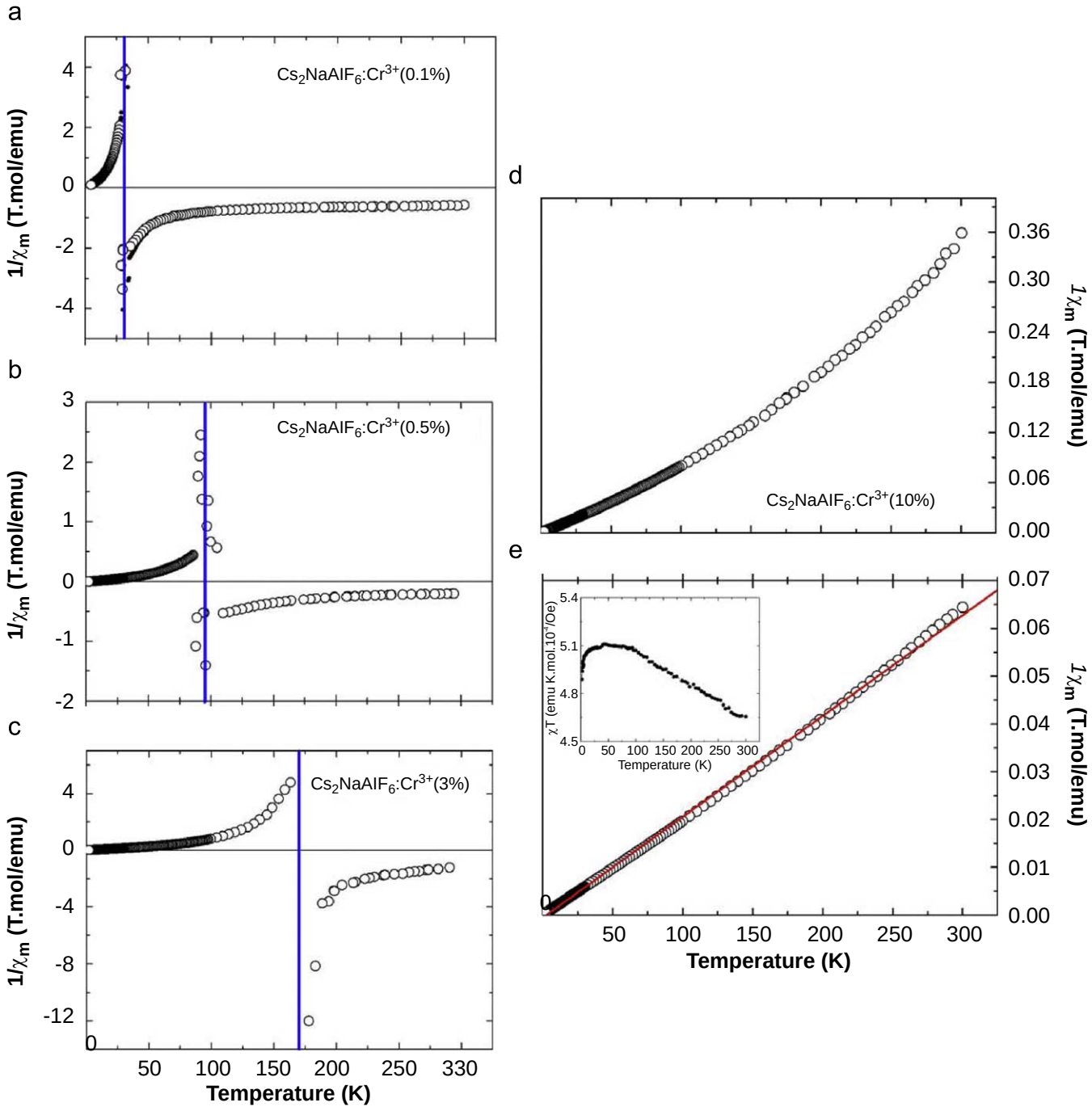

Fig. 5. Temperature dependence of the reciprocal magnetic susceptibility for Cs_2NaAlF_6 with (a) 0.1, (b) 0.5, (c) 3, (d) 10 and (e) 50 at% Cr^{3+} measured in 1 kOe. The inset of the figure χT vs. T gives further evidence of antiferromagnetic correlations between the Cr^{3+} ions for the 50 at% Cr^{3+} sample.

The ensemble of our results suggests that chromium ions are not magnetically isolated [30–32], however, the chromium content does not exceed the "percolation threshold" and long-range magnetic ordering is not observed. Furthermore, the $M(H)$ curves, obtained at 2 K and shown in Fig. 6, corroborates with the idea of magnetic domains. Magnetization curves (M–H) were found rigorously identical for all samples excluding the 0.1 at% Cr^{3+}, where a small hysteresis phenomena was observed. Within the diluted systems scenario with various strengths of AFM interactions, the M–H results can be well understood: "weak" AFM domains can be destroyed at a certain temperature and specific field, i.e. the spins can be flipped; in contrast, "strong" AFM domains will overcome the field-induced ferromagnetism. Indeed, for 0.1 at% Cr^{3+}at 2 K and $H > 1$ T, the AFM state is destroyed. Similar effect has been observed in doped manganites [33–35].

4. Conclusions

Based on our results even with very low-doping concentration of Cr^{3+}, a local mode that appears as a small wing to the A_{1g} mode indicates that the Cs_2NaAlF_6 host lattice is only locally perturbed. Indeed, no shift of the vibrational mode involving the AlF_6^{3-}

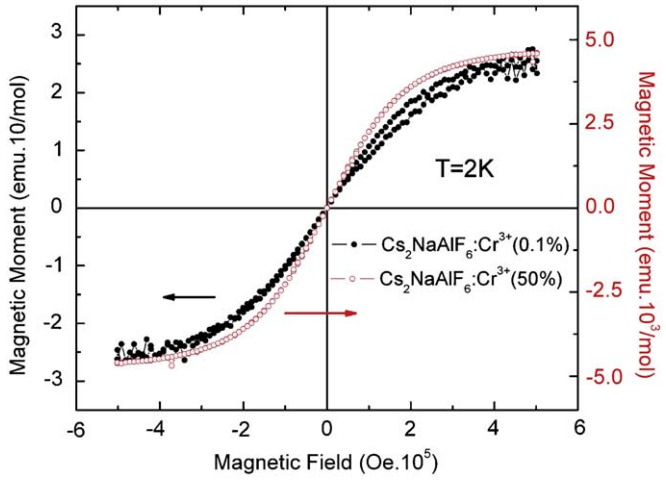

Fig. 6. Applied magnetic field dependence of the magnetization for Cs_2NaAlF_6 with 0.1 and 50 at% Cr^{3+} measured at 2 K. As the curves for the other compositions are identical, they were not shown. Note the small hysteresis for the 0.1 at% Cr^{3+} sample.

polyhedron as a function of doping level could be observed and no infrared signal became active. Perhaps most interesting to note is that the combination of broad and intense emission bands with a high quantum yield suggests that this system could be used as a wide band tunable light source, depending on the excitation wavelength.

The Curie magnetic moments for the 0.1, 0.5 and 3 at% Cr^{3+} samples rise with decreasing temperature and the diamagnetic contribution of the host lattice is overcome. For the 10 and 50 at% Cr^{3+} samples, we observe a Curie magnetization giving a spin state $S=\frac{1}{2}$ that is related to the trigonal distortion of the site. The question that remains to be answered is for which particular composition both quantum yield and magnetic effects are maximized. These studies are now underway. Furthermore, it is equally important to obtain information in the pure Cr^{3+} system. Although such a crystal is not easy to obtain, our group is now pursuing such growth.

Acknowledgements

FAPERJ is gratefully acknowledged for financial support of the authors. The authors wish to thank K. M. Hanif for the Raman measurements and Walter Kalceff (UTS-Sydney), Laurie Aldridge (ANSTO), Dimitri N. Argyriou and Simon Kimber (HZ Berlin) for discussions. We would also like to thank the anonymous reviewer of this paper for his/her constructive and judicious suggestions.

References

[1] R.H. Bartram, G.R. Wein, D.S. Hamilton, J. Phys: Condens. Matter 13 (2001) 2363.
[2] N. Shiran, A. Gektin, S. Neicheva, V. Voronova, V. Kornienko, K. Shimamura, N. Ichinose, Radiat. Meas. 38 (2004) 459.
[3] M.A.F.M. Silva, R.B. Barthem, L.P. Sosman, J. Solid State Chem. 179 (2006) 3718.
[4] O.S. Wenger, H.U. Güdel, J. Chem. Phys. 114 (2001) 5832.
[5] M. Grinberg, A. Suchocki, J. Lumin. 125 (2007) 97.
[6] G.C. Santana, A.C.S. de Mello, M.E.G. Valério, Z.S. Macedo, J. Mater. Sci. 42 (2007) 2231.
[7] G. Lakshminarayana, S. Buddhudu, Spectrochim. Acta Part A: Mol. Biomol. Spectrosc. 63 (2006) 295.
[8] M. Benabdesselam, P. Iacconi, E. Gheeraert, H. Kanda, D. Lapraz, D. Briand, Radiat. Prot. Dosimetry 100 (2002) 329.
[9] M.O. Ramirez, D. Jaque, M. Montes, J. Garcia Solé, L.E. Baisá, L. Ivleva, Appl. Phys. Lett. 84 (2004) 2787.
[10] H.N. Bordallo, R.W. Henning, L.P. Sosman, R.J.M. da Fonseca, A.D. Tavares Jr., K.M. Hanif, G.F. Strouse, J. Chem. Phys. 115 (2001) 4300.
[11] R.J.M. da Fonseca, L.P. Sosman, A.D. Tavares Jr., H.N. Bordallo, J. Fluoresc. 10 (2000) 375.
[12] H.N. Bordallo, X. Wang, K.M. Hanif, G.F. Strouse, R.J.M. da Fonseca, L.P. Sosman, A.D. Tavares Jr., J. Phys.: Condens. Matter 14 (2002) 12383.
[13] H. Vrielinck, F. Loncke, F. Callens, P. Matthys, N.M. Khaidukov, Phys. Status Solidi (c) 2 (2005) 384.
[14] J. Darriet, J.M. Dance, A. Tressaud, J. Solid State Chem. 54 (1984) 29.
[15] A.V. Goryunov, A.I. Popov, N.M. Khaidukov, Mater. Res. Bull. 27 (1992) 213.
[16] D.L. Rousseau, R.P. Bauman, S.P.S. Porto, J. Raman Spectrosc. 10 (1981) 253.
[17] A.G. Kalampounias, G.N. Papatheodorou, Z. Naturforsch. 62a (2007) 169.
[18] A. Chrissanthopoulos, G.N. Papatheodorou, J. Mol. Struct. 892 (2008) 93.
[19] P.A. Tanner, L. Yulong, N.M. Edelstein, K.M. Murdoch, N.M. Khaidukov, J. Phys.: Condens. Matter 9 (1997) 7817.
[20] U. Sliwczuk, R.H. Bartram, D.R. Gabbe, B.C. McCollum, J. Phys. Chem. Solids 52 (1991) 357.
[21] S.N. Krylova, A.N. Vtyurin, A. Bulou, A.S. Krylov, N.G. Zamkova, Phys. Solid State 46 (2004) 1311.
[22] A. Zoppi, C. Lofrumento, E.M. Castellucci, Ph. Sciau, J. Raman Spectrosc. 39 (2008) 40.
[23] L.P. Sosman, A. Dias Tavares Jr., R.J.M. da Fonseca, T. Abritta, N.M. Khaidukov, Solid State Commun. 114 (2000) 661.
[24] K. Nakamoto, Infrared Spectra of Inorganic and Coordination Compound, Wiley, New York, 1963.
[25] S.E. Stokowski, A.L. Schawlow, Phys. Rev. B 178 (1969) 457.
[26] B. Di Bartolo, Optical Interaction in Solids, Wiley, New York, 1968.
[27] I.V. Chepeleva, E.A. Zhilinskaya, V.N. Lazukin, A.P. Chernov, Phys. Status Solidi (b) 73 (1976) 65.
[28] E. Fawcett, Rev. Mod. Phys. 60 (1988) 209.
[29] C. Rudowicz, M.G. Brik, N.M. Avram, Y.Y. Yeung, P. Gnutek, J. Phys.: Condens. Matter 18 (2006) 5221.
[30] I. Ardelean, M. Peteanu, V. Simon, C. Bob, S. Filip, J. Mater. Sci. 33 (1998) 357.
[31] H.N. Bordallo, L. Chapon, J.L. Manson, J. Hernandez-Velasco, D. Ravot, W. Reiff, D.N. Argyriou, Phys. Rev. B 69 (2004) 224405.
[32] H.N. Bordallo, L.P. Aldridge, G. Jock Churchman, W.P. Gates, M.T.F. Telling, K. Kiefer, P. Fouquet, T. Seydel, S.A.J. Kimber, J. Phys. Chem. C 112 (2008) 19982.
[33] S.C. Bhargava, H.P. Kunkel, S. Singh, S.K. Malik, D.D. Buddhikot, A.H. Morrish, Phys. Rev. B 71 (2005) 104419.
[34] Li Pi, J. Cai, Q. Zhang, S. Tan, Y. Zhang, Phys. Rev. B 71 (2005) 134418.
[35] S. Karmakar, S. Taran, B.K. Chaudhuri, H. Sakata, C.P. Sun, C.L. Huang, H.D. Yang, Phys. Rev. B 74 (2006) 104407.